

Channel planform geometry and slopes from freely available high-spatial resolution imagery and DEM fusion: Implications for channel width scalings, erosion proxies, and fluvial signatures in tectonically active landscapes

G. Burch Fisher ^{a,*}, Bodo Bookhagen ^b, Colin B. Amos ^c

^a Department of Earth Science, University of California, Santa Barbara, CA, 93106, United States

^b Department of Geography, University of California, Santa Barbara, CA, 93106, United States

^c Department of Geology, Western Washington University, Bellingham, WA, 98225, United States

ARTICLE INFO

Article history:

Received 31 January 2013

Received in revised form 8 April 2013

Accepted 9 April 2013

Available online 15 April 2013

Keywords:

Google Earth

Lidar

ASTER GDEM

SRTM

Specific stream power

ABSTRACT

The rapid expansion of high-spatial resolution optical sensors and imagery over the last decade presents exceptional opportunities for quantifying visible attributes of geomorphic systems. In this study, we detail a simple, robust methodology (ChanGeom) to extract continuous channel width and centerline datasets for single-thread channels using freely available high-spatial resolution imagery currently available in Google Earth and Bing Maps. Comparisons with a global dataset of field and lidar-derived channel widths indicate minimal errors associated with the imagery and ChanGeom methodology (<1% overall), while examples from the Goriganga River (Indian Himalaya) and the Yakima River (WA, USA) emphasize the benefit of empirical width values over established channel width scalings in deciphering fluvial responses to complex landscape forcings in tectonically active regions. Additionally, accurate centerline delineation from the ChanGeom methodology provides improved sinuosity measurements, and when fused with coarse resolution digital elevation models (DEMs), removes along-profile shortening and coincident increases in reach-scale channel slope. Lastly, comparisons of ASTER GDEM V2, SRTM V4.1, and lidar channel profiles extracted in moderate to high-relief regions demonstrate the inferiority of the ASTER GDEM for channel slope calculations, despite the apparent spatial resolution advantages (9×). The methodology presented here will facilitate new discoveries in the fluvial environment that have historically been difficult due to access and imagery resolution issues, and provide greater perspective on channel signatures and responses to a host of landscape forcings, especially in tectonically active bedrock and lower order drainage systems.

© 2013 Elsevier B.V. All rights reserved.

1. Introduction

Scaling-relationships among channel slope, width, and discharge/drainage area are well-documented for graded rivers and remain as integral parameters in quantifying a host of hydraulic, geomorphic, tectonic, and ecological relationships in fluvial systems (e.g., Leopold and Maddock, 1953; Hack, 1957; Knighton, 1998). In non- or quasi-equilibrium fluvial systems, specifically tectonically active regions, many of the established scaling rules break down and are complicated by complex faulting, differential uplift regimes, lithologic variability, and a host of geomorphic processes (e.g. landsliding, outburst floods, glacial scouring) (Duvall et al., 2004; Whittaker et al., 2007; Yanites et al., 2010; Fisher et al., 2012). Furthermore, many active orogenic zones are located in remote locations where field access is both cumbersome and expensive. With the advent of globally available digital elevation models over the last decade, the geomorphology community has progressed considerably in its ability to quantitatively

link channel slopes to tectonic rates in well-constrained systems, as well as extract relative approximations of tectonic rates over larger spatial scales (Seeber and Gornitz, 1983; Kirby and Whipple, 2001; Wobus et al., 2006a; Kirby and Whipple, 2012). In contrast, overall understandings of channel geometry (i.e. width and depth) response to tectonic, lithologic, climatic, and geomorphic forcings have been incremental, and to date, predominately relied on numerical models (Stark, 2006; Wobus et al., 2006b; Attal et al., 2008; Turowski et al., 2009), flume studies (Turowski et al., 2006; Finnegan et al., 2007), and limited empirical observations (Lavé and Avouac, 2001; Snyder et al., 2003; Duvall et al., 2004; Amos and Burbank, 2007; Craddock et al., 2007; Whittaker et al., 2007; Snyder and Kammer, 2008; Wohl and David, 2008; Jansen et al., 2010; Yanites et al., 2010; Kirby and Ouimet, 2011; Whipple et al., 2013). Progress with regard to predicting channel width and depth evolution in tectonically active regions has been further hindered by the difficulty in constraining sediment transport conditions, which can greatly influence channel geometries (Whipple, 2004; Turowski et al., 2007; Yanites and Tucker, 2010; Whipple et al., 2013) and make simple channel width predictions in complex orogenic systems difficult.

* Corresponding author.

E-mail address: burch@eri.ucsb.edu (G.B. Fisher).

Passive optical satellite and aerial imagery, on the other hand, has been used for decades to quantify river form and process across a broad range of geomorphic settings (Smith, 1997; Marcus and Fonstad, 2008; Smith and Pavelsky, 2008). Until recently, however, remote measurements of channel geometry have been limited by the spatial resolution of satellite imagery and/or the availability of aerial photos, thereby restricting analyses to larger channel systems and/or more developed geographic regions. Whereas our understanding of large-scale channel dynamics and geometric scalings has greatly benefitted from remotely-sensed imagery, there remains a dearth of complimentary empirical data on lower-order alluvial and bedrock systems common in active mountain belts. The last decade, however, has seen a vast expansion of publicly available, online, high-spatial resolution satellite systems (e.g., IKONOS, GeoEye, DigitalGlobe, CNES/Spot), as both technological and economic hurdles have been overcome (Fisher et al., 2012). This expansion has resulted in the availability of high-spatial resolution imagery (<1 to 5 meter horizontal resolutions) across much of the globe as well as simplified distribution hubs and interactive platforms (e.g., Google Earth, Microsoft Bing Maps) (Fisher et al., 2012). For researchers in the fluvial domain, widespread high-spatial resolution imagery enables new research ventures into channel processes and form at spatial scales and in geographic locations that were previously impossible.

In this paper we use high-spatial resolution satellite and aerial imagery freely available through Google Earth and Bing Maps in ArcGIS 10 to demonstrate the benefits of using such imagery to better quantify river planform geometry (width and sinuosity), erosion proxies, and channel width response to geomorphic, lithologic, and tectonic processes in tectonically active regions. To this end, we present a simple, robust methodology (ChanGeom) to estimate channel planform, centerline, and width values from freely available high-spatial resolution imagery and compare the results with a globally distributed dataset of field- and lidar-derived channel width values. In addition, we present a methodology for fusing coarse resolution DEMs to the high-resolution channel centerline derived from the ChanGeom methodology, in order to diminish channel shortening and improve overall channel reach-scale slope estimates. These results are then compared with data from the 30-m Advanced Spaceborne Thermal Emission and Reflectance Global Digital Elevation Map (ASTER GDEM) (Slater et al., 2011), 90-m Shuttle Radar Topography Mission (SRTM) (Farr et al., 2007), and airborne lidar derived estimates. Lastly, we discuss the benefits and caveats of using these methodologies, through real world examples, for improving current understandings of channel geometry scalings, erosional proxies, and landscape processes in tectonically active orogens.

2. Background

2.1. Slope and width scalings

Channel slope scalings have been well approximated for years in graded profiles based on empirical observations (Mackin, 1948) and formulations (Hack, 1957) where channel slope (S) scales as a power-law relationship with drainage area (A) to an exponent ($-\theta$), defined as the concavity index, multiplied by the channel steepness index (k_s).

$$S = k_s A^{-\theta} \quad (1)$$

This equation, though simplistic, allows for variable climatic, tectonic, and lithologic regimes through manipulation of the concavity index exponent and the channel steepness index parameter. With the advent of nearly global digital elevation models over the last two decades, direct approximations of channel slopes in graded and non-graded fluvial networks have become routine, with considerable progress made using channel steepness indices derived from Eq. (1)

to quantify tectonic rates (cf. Wobus et al., 2006a; Kirby and Whipple, 2012). Despite the ability to directly quantify channel slopes from digital elevation models, the accuracy of such endeavors greatly depends on the digital elevation model's spatial resolution, procurement system, signal smoothing algorithms, and the channel profile extraction methodology. Whereas high-spatial resolution lidar-derived DEMs will produce very accurate slope estimates over relatively short length scales, considerable channel shortening and over-steepened slopes have been documented when using coarser, near global datasets like the 30-m ASTER GDEM and 90-m SRTM (Allen et al., 2011; Passalacqua et al., 2012).

In contrast to channel slope, channel width cannot be directly measured in a large percentage of global channel networks from DEMs, with the exception of large mainstem rivers (e.g. lower reaches of the Ganges and Amazon rivers) or using high-spatial resolution DEMs (e.g. 1-m lidar). The inability to easily measure channel widths from DEMs has forced geomorphologists to rely on sparse field-measurements, remotely sensed imagery, and/or scaling relationships formulated from graded equilibrium profiles (Leopold and Maddock, 1953). Generally, channel width (W) is thought to scale in a power-law relationship with mean annual discharge (Q) to an exponent (b) times a constant (a) that is unique to the hydrometeorology of the watershed.

$$W = aQ^b \quad (2)$$

In both bedrock and alluvial channel systems the exponent (b) has been shown to range between 0.3 and 0.6, with 0.5 as the most commonly used value (Knighton, 1998; Montgomery and Gran, 2001; Whipple, 2004; Wohl and David, 2008; Whipple et al., 2013). Eq. (2) can also be specified with respect to contributing area (A) instead of discharge (Q), which has been shown to yield (b) values between 0.4 and 1 (Wohl and David, 2008). While the power-law scaling approach has generally been successful in capturing “average” width behavior across a host of tectonically active and quiescent landscapes (Montgomery and Gran, 2001; Craddock et al., 2007; Wohl and David, 2008; Yanites et al., 2010; Kirby and Ouimet, 2011; Whipple et al., 2013), both empirical and theoretical models show that such simplifications fail to adequately represent channel geometry responses to tectonic, lithologic, and geomorphic forcings (Duvall et al., 2004; Turowski et al., 2006; Amos and Burbank, 2007; Whittaker et al., 2007; Yanites and Tucker, 2010; Yanites et al., 2010).

Acknowledging the limitations of the power-law approximations of channel width, attempts to derive more comprehensive models and frameworks to predict channel geometry have been proposed. The most widely cited of these formulations combines the empirically derived Manning's equation with principles of mass conservation to yield a relationship between width (W) (m), the width-to-depth ratio (α) (m m^{-1}), discharge (Q) ($\text{m}^3 \text{s}^{-1}$), channel slope (S) (m m^{-1}), and Manning's roughness coefficient (n) (Manning, 1891; Finnegan et al., 2005).

$$W = \left[\alpha(\alpha + 2)^{2/3} \right]^{3/8} Q^{3/8} S^{-3/16} n^{3/8} \quad (3)$$

Whereas this model attempts to predict the dynamic response of channels by accounting for the coevolution of multiple channel parameters, the added complexity produces even more free parameters in unconstrained and remote channel systems that makes accurate channel prediction nearly impossible (Fisher et al., 2012). In addition, this model relies on the assumptions of the channel being in steady-state and neglects the well-documented effects of landscape transience (cf. Whittaker et al., 2007) and sediment transport and cover variability on channel geometries (Johnson and Whipple, 2007; Turowski et al., 2007; Yanites and Tucker, 2010). More comprehensive ‘optimized’ models have been developed to encompass the

interactions between channel geometry and sediment and uplift regimes, however, the predictive ability and benefits of such models remain a posteriori in most cases and require knowledge of an even greater number of parameters as well as equilibration with local forcing variables (Turowski et al., 2007; Yanites and Tucker, 2010).

2.2. Specific stream power erosion proxy

Specific stream power incorporates channel width into models for fluvial erosion through a simple physics-based proxy for work performed on the bed of a channel and is defined as the energy expended on a unit area of the channel bed for a given flow (Bagnold, 1960, 1977). In its most simplistic form specific stream power (ω) (W m^{-2}) relates the energy expended on the bed of the channel to the specific weight of water (ρg) ($\sim 9810 \text{ N m}^{-3}$), the width of the channel (W) (m), the discharge (Q) ($\text{m}^3 \text{ s}^{-1}$), and the energy slope, often approximated by the bed slope (S) (m m^{-1}).

$$\omega = \rho g Q S / W \quad (4)$$

This simple, but insightful, equation has been used to infer a wide range of fluvial processes ranging from exhumation and erosion rates (Whipple et al., 2000; Whipple, 2004; Yanites et al., 2010; Bookhagen and Strecker, 2012) to flood power (Magilligan, 1992), to sediment and wood stability (Bagnold, 1977; Fisher et al., 2010) in fluvial systems. Along with channel steepness indices, specific stream power provides one of the few quantifiable erosion/tectonic rate proxies in remote orogenic systems. To date, however, specific stream power approximations have mostly relied on power-law approximations to produce width values (Eq. (2)), yielding little more insight than that provided by channel steepness indices alone (Eq. (1)).

2.3. Freely available imagery

Remotely sensed optical imagery has been used for decades to quantify river characteristics but has been limited in its applicability by the effective spatial resolution of many of the globally distributed systems, such as multispectral sensors like Landsat (15 and 30 m horizontal resolutions) and ASTER (15 m horizontal resolution). Over the last decade many of these older systems have been overshadowed by a rapid expansion of high-spatial resolution optical sensors (<1 to 5 m horizontal resolution). These powerful new systems have permeated every segment of society, but are aimed at a commercial market with high end-user costs. Recognizing the value of such imagery in furthering their business models, both Google and Microsoft have invested heavily in providing freely available visible imagery to the public. Through Google Earth users can scan both global spatial and temporal archives of high-spatial resolution imagery (<1 to 5 m horizontal resolution) as well as spatially interact with the data using georegistered digitization and export capabilities (Fisher et al., 2012). Microsoft Bing Maps, on the other hand, has proprietary high-spatial resolution aerial imagery (<1 m horizontal resolution) available across the United States, which can be currently interacted with for free in the ArcGIS 10 environment. In contrast with multispectral datasets, digitization is the only way to obtain information from the imagery, since no spectral or band interaction is currently available to the user. Furthermore, little is known about how the imagery is collected, orthorectified, merged, and filtered as these are proprietary to both Google and Microsoft. Previous work using Google Earth imagery, however, attests to the general accuracy both in spatial location as well as in proportions and distances when compared to field data (Potere, 2008; Fisher et al., 2012; Tewksbury et al., 2012). For a comprehensive overview of the imagery types, applications, benefits, and caveats associated with using Google Earth to study earth surface processes see Fisher et al. (2012).

3. Methodology

3.1. Channel geometry from high-spatial resolution imagery (ChanGeom)

The ChanGeom algorithm is an optimized routine for quantifying single-thread channel planform geometries (channel centerline and width values) from digitized or spectrally extracted polygons and provides a robust and rapid Matlab alternative to complimentary IDL (Pavelsky and Smith, 2008) and lidar extraction techniques (McKean et al., 2009; Passalacqua et al., 2012). The major benefit of the ChanGeom algorithm over the IDL-based RivWidth algorithm (Pavelsky and Smith, 2008) is in the computational efficiency in measuring single-thread channels and a greater working knowledge and adoption of Matlab over IDL in the geomorphology community. The efficiency is aided by sophisticated image processing functions available in the Matlab environment, which allow rapid polygon thinning and width measurement. This is in contrast to the more computationally intensive centerline orthogonal cross sections utilized in RivWidth. That being said, the added complexity of the RivWidth code results in enhanced capabilities, including measuring single-thread and braided systems as well as quantifying multiple interconnected tributaries in a single run. Both ChanGeom (see the Appendix A) and RivWidth (<http://www.unc.edu/~pavelsky/Pavelsky/RivWidth.html>) algorithms are made freely available online, however, we acknowledge that both Matlab and IDL licensing costs are not trivial. In addition, the ChanGeom algorithm currently requires the Image Processing Toolbox, which adds additional costs to a basic Matlab license, but is currently included in student licenses. Given this, we plan to transfer the ChanGeom code entirely to Python as soon as comparable image processing routines are available, effectively making the entire ChanGeom methodology completely free for all users.

For each of the case studies presented in this paper, detailed single-thread bankfull channel margins were digitized in Google Earth (with “terrain” mode off) and Bing Maps in ArcGIS 10 using freely available high-spatial resolution true color imagery (SPOT, DigitalGlobe, GeoEye, aerial images) with channel margins identified by any combination of high water marks, lack of vegetation, rock staining, scoured lateral bars, surface textures, etc. (Fig. 1; Table 1) (Leopold and Maddock, 1953; Knighton, 1998; Whipple, 2004; Fisher et al., 2012). Due to the nature of the freely available Google Earth and Bing Maps imagery utilized in this study, spectrally based extraction methodologies are precluded, requiring more labor intensive hand-digitizing. Despite this, on average between 10 and 25 km of channel length can be digitized per hour allowing sizable lengths of river to be covered in a relatively short period of time. Digitized polygons were then exported as KML files and imported into a geographic information system where they were rasterized into a channel mask using a cell size of at least one-third of the width of the narrowest section of the channel reach to ensure accurate width values throughout (Fig. 2). While actual width accuracy can never be greater than the resolution of the imagery from which it is acquired, the algorithm requires at least three pixels across the channel to produce a value, which is the basis for the 1/3 rule. In addition, the value chosen for the raster resolution will set both the intrinsic error and the processing efficiency of the algorithm, and should be chosen carefully (see Section 4.1). Next, the rasterized channel mask is thinned one pixel at a time along the channel mask until a channel centerline one pixel wide is created (Lam et al., 1992). The algorithm then calculates a quasi-Euclidean distance from each centerline pixel to the channel mask margins, producing a half-width value that is then multiplied by two to yield the channel width at each centerline pixel (Breu et al., 1995). The rasterized centerline with channel width information is then vectorized to enable spatial merging with other datasets. Additional implementation details can be found in the user’s manual and Matlab source code (see Appendix A for download details).

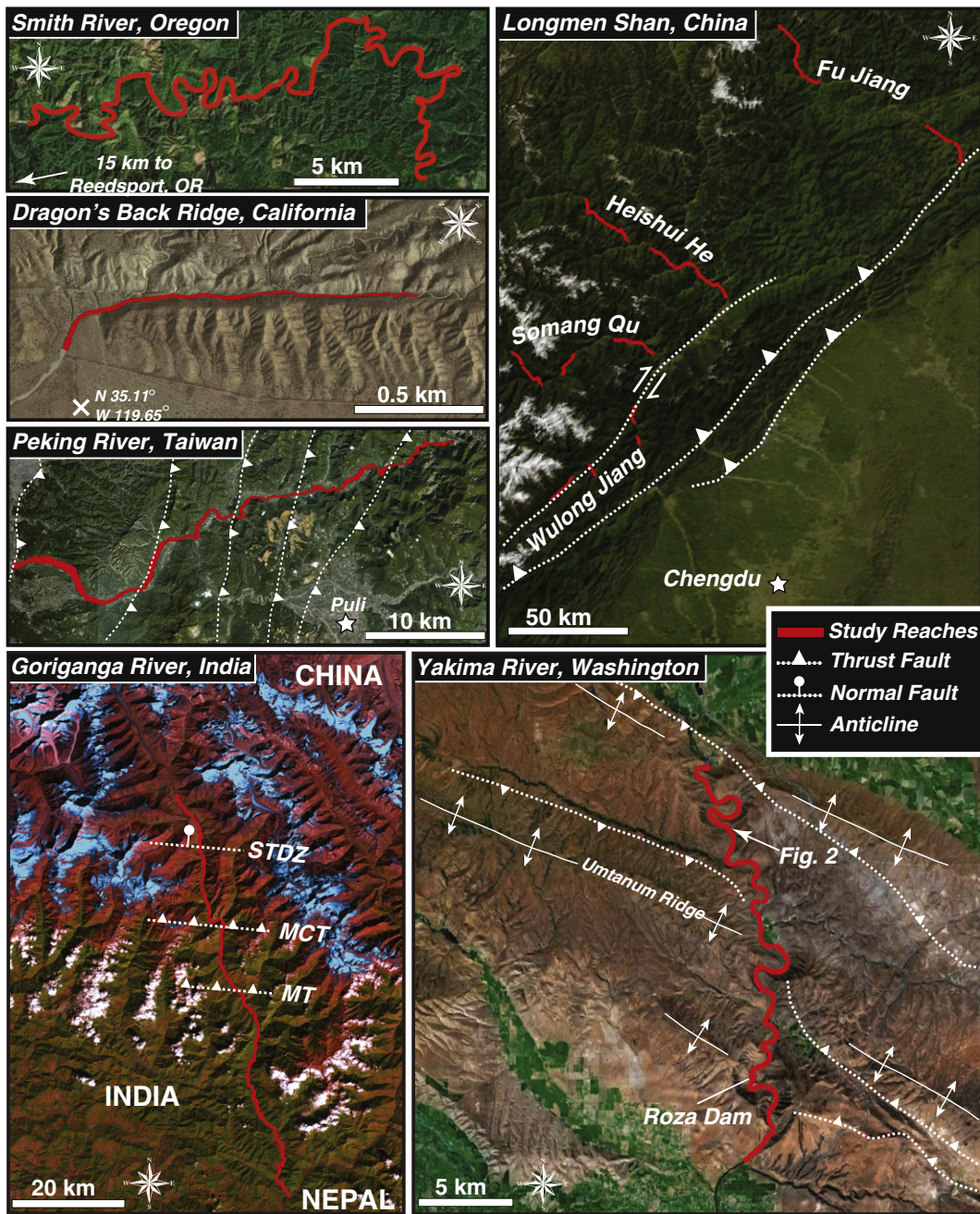


Fig. 1. River reaches (red) used in this study with major tectonic structures detailed.

In order to test the accuracy of the ChanGeom methodology and the imagery used within Google Earth and Bing Maps, results from the ChanGeom algorithm were compared to both field and airborne lidar (light detection and ranging) datasets from tectonically active regions as detailed below.

3.2. Comparison with field data

Field-measured channel width datasets from the Peking River, Taiwan (Yanites et al., 2010) and the Longmen Shan, China (Kirby and Ouimet, 2011) were used to assess the accuracy of the ChanGeom methodology as well as the imagery underlying the analysis. In total, 52.5 km (22,500 width measurements) of the Peking River and 237.3 km (100,369 width measurements) of river in the

Longmen Shan were digitized and processed using a raster resolution of 2 m (Fig. 1). These datasets were then compared to 142 suitable corresponding field measurements taken along the Peking River ($n = 55$) (Yanites et al., 2010) and in the Longmen Shan ($n = 87$) (Kirby and Ouimet, 2011). At each field-width measurement site a line perpendicular to flow was drawn orthogonal to flow across the river and the closest value within a 10-m radius of the intersection with the ChanGeom centerline was recorded. Suitable sites were defined by clear delineation of both channel margins (i.e. no shadowing or clouds), unambiguous GPS point locations from the field measurements, lack of significant anthropogenic or natural channel augmentation postdating field collection and predating the available imagery (e.g. Wenchuan earthquake), field widths of less than 200 m (due to the limits of the laser rangefinders used in both field

Table 1
Imagery types, approximate collection dates^a, and sources used in this study.

Study river	Type of imagery	Date of imagery	Source
Dragon's Back, CA	GeoEye	12-Sept-2009	Google Earth
Smith River, OR	Aerial photo	29-Jun-2005	Bing Aerial Images in ESRI ArcGIS 10
Yakima River, WA	Aerial photo	3-Sept-2011	Google Earth
Goriganga River, India	DigitalGlobe, GeoEye, CNES/Spot	2000, 2005, 2009	Google Earth
Longmen Shan, China	DigitalGlobe, GeoEye, CNES/Spot	2002, 2003, 2005, 2008, 2010	Google Earth
Peking River, Taiwan	DigitalGlobe, GeoEye, CNES/Spot	2003, 2006, 2010	Google Earth

^a Imagery collection dates are approximate and based only on the information provided by Google Earth. In general, GeoEye and Digital Globe dates appear to be robust while CNES/Spot imagery dates provided by Google Earth remain suspect.

studies), and reaches devoid of abrupt width changes, where field GPS errors on the order of tens of meters might cause large discrepancies in recorded channel width values.

3.3. Comparison with lidar datasets

In order to demonstrate the robustness of the ChanGeom methodology across a large range of channel widths (~1 to 150 m) and a greater number of measurements and channel types, we compared channel widths derived from both freely available imagery and lidar datasets using the ChanGeom method. Channel margins were delineated in lidar datasets along an ephemeral stream draining the Dragon's Back Pressure Ridge, California (collected in May 2005 by the National Center for Airborne Laser Mapping, NCALM) and along the Yakima River in southeast Washington state (collected in April 2007 by NSF Earthscope) (Fig. 1) by creating both hillshade and

slope maps to identify abrupt channel margin topographic transitions marking the hillslope-channel boundary. In total, 1.5 km of channel (5550 points at a resolution of 0.2 m) along the Dragon's Back Ridge and 38.1 km (16,054 points at a resolution of 2 m) along the Yakima River were digitized and processed using the ChanGeom methodology from both high-spatial resolution imagery and the 1-m resolution lidar datasets. In order to compare the datasets, where minor centerline offsets are inevitable, the lidar width value spatially closest to each imagery-derived width value was joined allowing easy comparison of the two datasets (using the method shown in Fig. 3).

3.4. Channel slope comparison

Approximately 50 km of channel length along the Smith River in Oregon was digitized using a raster resolution of 2 m (21,651 channel width measurements) in order to quantify and rectify channel shortening associated with using coarse resolution global DEM datasets (Fig. 1). Both 90-m SRTM V4.1 (Farr et al., 2007; Jarvis et al., 2008) and 30-m ASTER GDEM V2 (Slater et al., 2011) datasets were processed for the study reach using a D8 flow routing algorithm to produce channel elevation datasets (O'Callaghan and Mark, 1984). The SRTM and ASTER GDEM datasets were both merged to the ChanGeom centerline data (imagery + DEM fusion) and used unfused in order to quantify shortening as compared to the 2-m lidar dataset (Fig. 3). The lidar dataset was also merged with the ChanGeom centerline in order to prevent intra-channel sinuosity derived from the simplified flow algorithm and the comparatively small pixel size-to-channel width ratio. Fused and unfused longitudinal profiles were then smoothed using a 5-km moving average kernel, while the lidar dataset was smoothed using a 1-km smoothing kernel to remove any high-frequency noise. The 5-km smoothing window was chosen due to good coherence with the lidar dataset and the lack of significant perturbations observed when using shorter smoothing kernels.

3.5. Widths and specific stream power along the Goriganga River, India

To demonstrate the benefits of using continuously measured widths along a tectonically active river profile as compared with simple power-law scalings, approximately 90 km of channel length

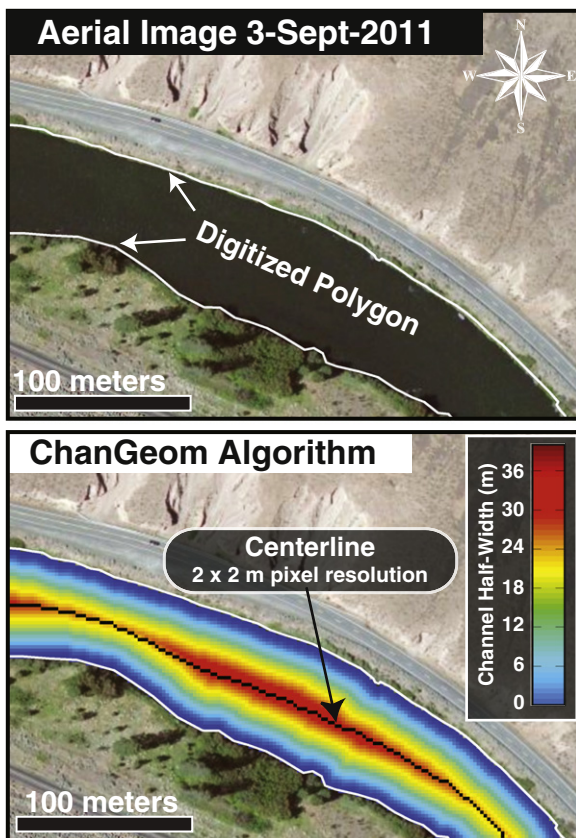


Fig. 2. Example of the ChanGeom algorithm performed on a polygon digitized from an aerial image (Google Earth) along the Yakima River study reach (see Fig. 1).

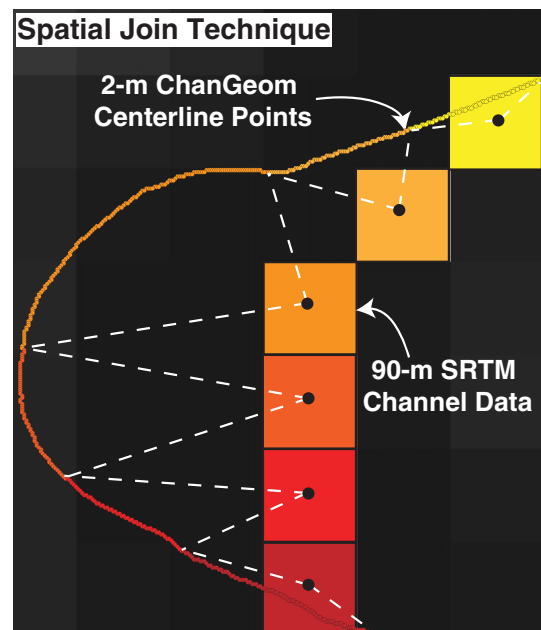


Fig. 3. Technique used to fuse/join two datasets of different resolution using the spatially closest point (e.g., SRTM elevation data to the ChanGeom centerline).

(27,033 width measurements at a raster resolution of 3 m) were digitized using the ChanGeom methodology along the Goriganga River in northern India in the western Himalaya (Fig. 1). This dataset crosses three of the major Himalayan tectonic structures (Munsiyari Thrust, Main Central Thrust, and South Tibetan Detachment Zone) that bound contrasting tectonic, lithologic (Lesser Himalayan Sedimentary, Lesser Himalayan Crystalline, High Himalayan Crystalline, and Tethyan Series) (Hodges, 2000), and geomorphic regimes (recently glaciated/unglaciated). For specific stream power (ω) calculations channel elevation profile data were derived from 90-m Shuttle Radar Topography Mission (SRTM) data and then spatially joined to the channel width dataset (Fig. 3). Both channel slopes and widths were smoothed using a 5-km moving average kernel to better illustrate general longitudinal trends. Mean annual discharge ($\text{m}^3 \text{s}^{-1}$) along the Goriganga River was derived from the average of a 10-year coupled snowmelt–rainfall–evapotranspiration hydrological model for the study area (Bookhagen and Burbank, 2010).

4. Results and discussion

4.1. ChanGeom and imagery accuracy, errors, and complicating factors

Comparisons of channel widths derived from freely available imagery using the ChanGeom algorithm with both field-measured and lidar-derived channel widths show high correlation (<1% deviation at 95% CI) and indicate no observable difference between individual high-spatial resolution products (GeoEye, DigitalGlobe, SPOT, aerial photos) (Fig. 4). These results provide confidence that both the imagery available in Google Earth (with terrain mode off) and Bing Maps are accurately processed and that the ChanGeom methodology provides robust results from the digitized polygons from this imagery. The main error intrinsic to the ChanGeom algorithm itself is the raster resolution used to convert the digitized polygon to a matrix. In this study an independently determined resolution of between 0.2 and 3 m was used (based on 1/3 the width of the narrowest section) to assure width values across all parts of each study reach. In general, the intrinsic ChanGeom width algorithm error will be equal to approximately one-third the raster resolution value (errors < 1 m in this study) and will depend on the specific polygon-to-raster conversion algorithm used. This value should be taken into account when deciding the appropriate raster resolution for a given project, though it is usually negligible when compared to most external errors and the spatial resolution of the imagery from which it is derived.

External errors will likely arise from variables that are unrelated to the ChanGeom algorithm such as imagery issues (spatial resolution, shadowing, warping, sensor look angle, orthorectification) (cf. Marcus and Fonstad, 2008; Fisher et al., 2012), obscured channel margins (due to riparian vegetation, anthropogenic augmentation, recent flooding, etc.) (Fig. 4C), and user error (channel margin delineation and digitizing accuracy). Each of these cases will depend on the quality of the imagery, the characteristics of the channel system, and the researcher's ability. In most cases the minimum channel width to which this technique can be applied will depend on the imagery resolution (<1 m to 5 m in this study), but factors such as riparian vegetation (e.g. Pacific northwest), clouds, and image warping may partially or completely obscure much wider channels and prevent certain locations and images from being used (Fig. 4C). Nevertheless, our data shows that, across a broad range of high-spatial resolution imagery types, geomorphic and tectonic locations, and channel characteristics the overall error associated with the ChanGeom algorithm remains quite low. This close agreement demonstrates the potential of freely available high-spatial resolution imagery to greatly improve and expand empirical datasets describing channel planform characteristics (e.g. width and sinuosity) and evolution with respect to a diverse range of landscape variables (e.g. varying lithologic, sediment, discharge, climate, and tectonic regimes).

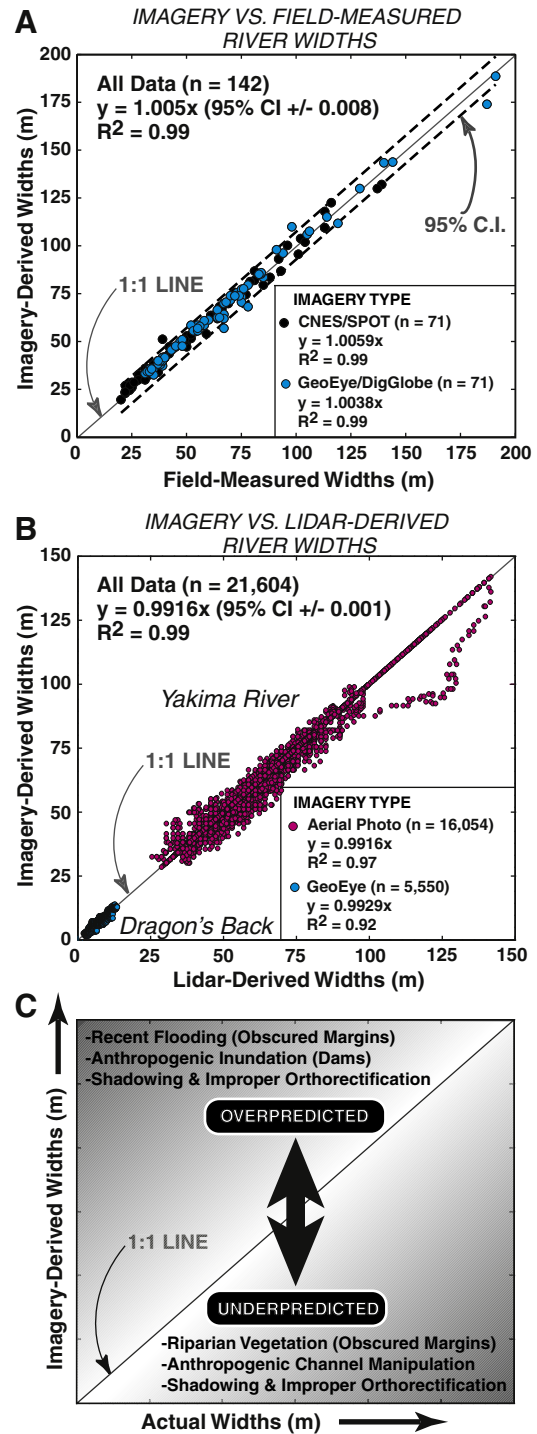


Fig. 4. ChanGeom imagery-derived widths compared with A) field-measured widths from Taiwan (Yanites et al., 2010) and the Longmen Shan, China (Kirby and Ouimet, 2011) and B) ChanGeom lidar-derived datasets from the Dragon's Back Ridge, CA and the Yakima River, WA. Note that most of the statistically insignificant noise in the lidar comparison is likely due to small-scale channel geometry evolution that occurred between the lidar acquisition (May 2005 – Dragon's Back Ridge; April 2007 – Yakima River) and that of the high-spatial resolution imagery (September 2009 – Dragon's Back; September 2011 – Yakima River). C) Conceptual diagram outlining potential mechanisms for under/overestimation of width values using high-spatial resolution imagery. Note that field-derived channel width measurements have inherent uncertainty as well and could similarly be affected. Note that all regressions were forced through the origin at (0,0).

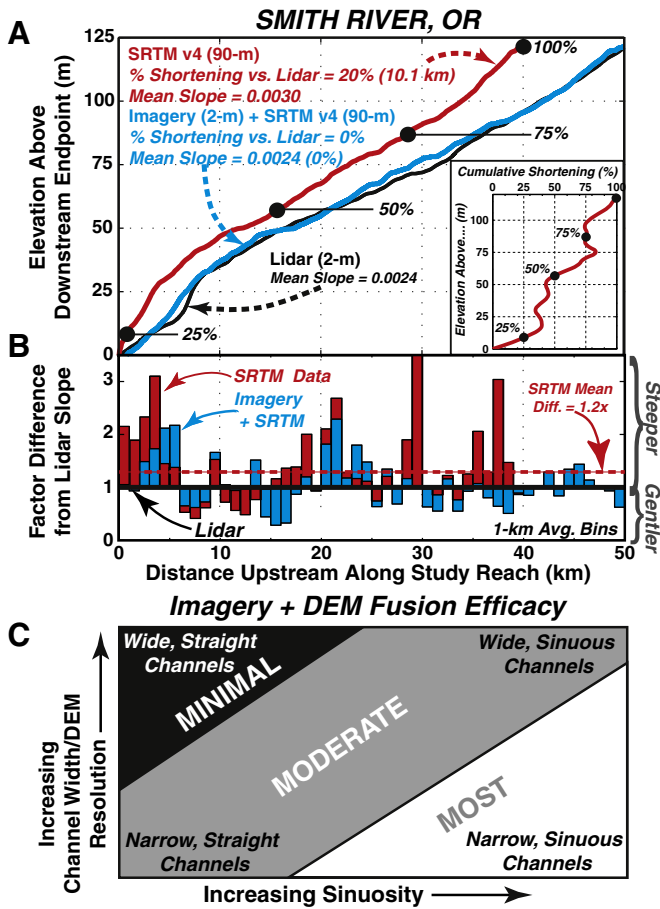


Fig. 5. A) Longitudinal profile data from 90-m SRTM, 2-m imagery + SRTM, and 2-m lidar datasets along the Smith River, OR. Inset shows cumulative shortening (%) versus elevation above the downstream endpoint for the SRTM dataset compared to that of the lidar. Note that 25% of the overall shortening occurs in the first few kilometers. B) Factor difference in 1-km binned channel slope values compared to lidar. Mean factor difference for SRTM is 1.2 or 20%, equal to the overall shortening of the SRTM dataset. Imagery + SRTM has a mean factor difference of 1, indicating no shortening when compared to the lidar dataset. C) Conceptual diagram showing where the imagery-DEM fusion will be most useful, though additional factors may play an important role (see Section 4.2).

4.2. Channel centerline applications and implications

The less obvious benefit of the ChanGeom methodology is the generation of a high-resolution channel centerline, which when fused with coarser DEMs can be used to improve quantification of both channel sinuosity and slopes. Channel sinuosity provides an integral metric for understanding the dynamics of channel meandering (Schumm and Khan, 1972; Schumm et al., 1972; Stølum, 1998) and oxbow lake formation (Constantine and Dunne, 2008) in alluvial reaches, and may act as a topographic signature recording variations in climate in actively incising systems (Stark et al., 2010). Yet, despite the importance of accurately determining sinuosity, in many locations it is often calculated using coarse DEMs and simplified flow algorithms (e.g. D8 – O’Callaghan and Mark, 1984). In contrast, accurate planform geometry can be achieved even in the most remote locations using the ChanGeom methodology, without the input of DEMs. The accurate delineation of a channel centerline from the ChanGeom algorithm permits calculation of robust sinuosity and should be especially valuable in smaller tributary and distributary networks, as well as low gradient systems where coarse DEMs can prove highly inaccurate at quantifying mainstem thalwegs.

Reach-scale channel slope measurements may also benefit from accurate centerline delineation by fusing the ChanGeom centerline with coarse elevation DEMs, such as the near global 90-m SRTM and 30-m ASTER GDEM datasets (Fig. 5) (Allen et al., 2011). Currently, much of the world relies on these two DEM datasets, even though these areas are usually covered by high-spatial resolution imagery. Data from the Smith River, Oregon shows the discrepancy between coarse resolution 90-m SRTM V4.1 data and 2-m lidar data where 20% channel shortening (apparent decrease in channel length of 10 km) is observed along the 50-km study reach, yielding coincident increases in apparent channel slopes (20% steeper). By fusing the ChanGeom centerline with the SRTM data, artifactual shortening is removed and more realistic slopes are produced across the study reach. Whereas noise always persists at the kilometer scale when compared to the lidar data, and results will partly depend on the amount and type of smoothing of the data, the overall pattern is greatly improved given the coarseness of the original SRTM data.

Where and to what extent channel shortening occurs depend on many factors including the ratio of channel width to DEM resolution (i.e. the DEM is too coarse to accurately track the river channel), sinuosity (i.e. straight channels are less likely to have shortening), valley

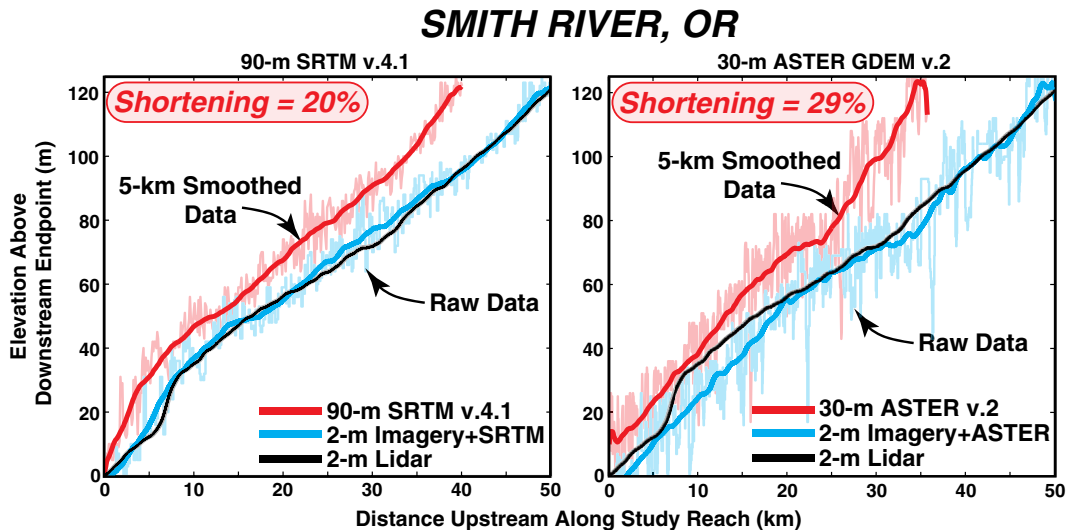


Fig. 6. Comparison of the 30-m ASTER GDEM V2 and 90-m SRTM V4.1 longitudinal profiles with that derived from the 2-m lidar data along the Smith River, OR. SRTM data displays considerably less noise and much better coherence with the lidar dataset than the ASTER GDEM, despite a 9 \times apparent resolution discrepancy. Imagery + SRTM fusion produces a reasonable match with the lidar data while imagery + ASTER data still fails to accurately depict the lidar results, even with considerable smoothing. Similar results are also found along the Yakima River.

width (i.e. the wider the valley the greater the ability for the channel to meander), the flow algorithm (i.e. the D8 algorithm will always take the shortest distance with the greatest vertical drop), and temporal discrepancies (i.e. changes may occur between the acquisition of the DEM and the imagery digitized) to name a few. The greatest benefits from the fusion technique, however, will generally occur when channel widths are smaller than the resolution of the DEM and sinuosity is high (Fig. 5C). Because channels in tectonically active landscapes tend to be steeper, and therefore less prone to meander, the greatest utility for the fusion technique is likely to be in intermediate (foreland systems) to lower slope channel systems (alluvial channels) with moderate to minimal tectonic influence. This finding is corroborated by preliminary work on mainstem Himalayan rivers

that finds channel shortening to be minimal between fused and unfused SRTM datasets (<5%) (Fisher et al., 2011).

Lastly, the considerable shortening and increased reach-scale slopes in the SRTM data compared to the lidar dataset indicate that caution should be applied when using these datasets to calculate channel-slope products and derivatives (e.g., channel steepness indices, shear stress, particle mobility, channel concavity). Furthermore, comparisons between ASTER GDEM V2 (Slater et al., 2011) and SRTM V4.1 (Farr et al., 2007; Jarvis et al., 2008) datasets along the Smith River study reach show the ASTER data to be both considerably noisier than SRTM data and completely incoherent with respect to the lidar data, even after considerable smoothing (Fig. 6). The considerable noise in the ASTER GDEM data has been documented by others in tectonically active regions (Allen et al., 2011) and is likely due to the limitations and constraints of the stereogrammetry process, the quality of the underlying imagery, the smoothing algorithms, and the amalgamation of temporally variable imagery at any given location. It is therefore recommended that studies utilizing coarse DEM channel slopes use the SRTM data (fused or unfused) preferentially over the ASTER GDEM in moderate to steep terrain. We acknowledge, however, that this recommendation may change with subsequent versions of the ASTER GDEM and the topographic characteristics of each location.

4.3. Channel width applications and implications

Channel width is a key hydraulic variable and/or boundary condition in nearly all channel flow equations and is essential for properly quantifying everything from discharge to sediment-transport capacity to erosion potential within a landscape (Leopold and Maddock, 1953; Knighton, 1998; Whipple, 2004; Smith and Pavesky, 2008). Despite this, channel width is almost never explicitly measured, especially in lower-order, tectonically active systems. The ChanGeom methodology enables efficient and explicit treatment of channel widths in both remote landscapes and at resolutions that were previously impossible using freely available imagery. Data from the Goriganga watershed in northern India demonstrates just how important the explicit treatment of channel widths can be in tectonically and lithologically variable settings (Fig. 7). Comparisons with both power-law scalings (Eq. (2)) and more complex width derivations (Eq. (3)) show considerable discrepancies that are consequently mirrored in the specific stream power erosion proxy calculations

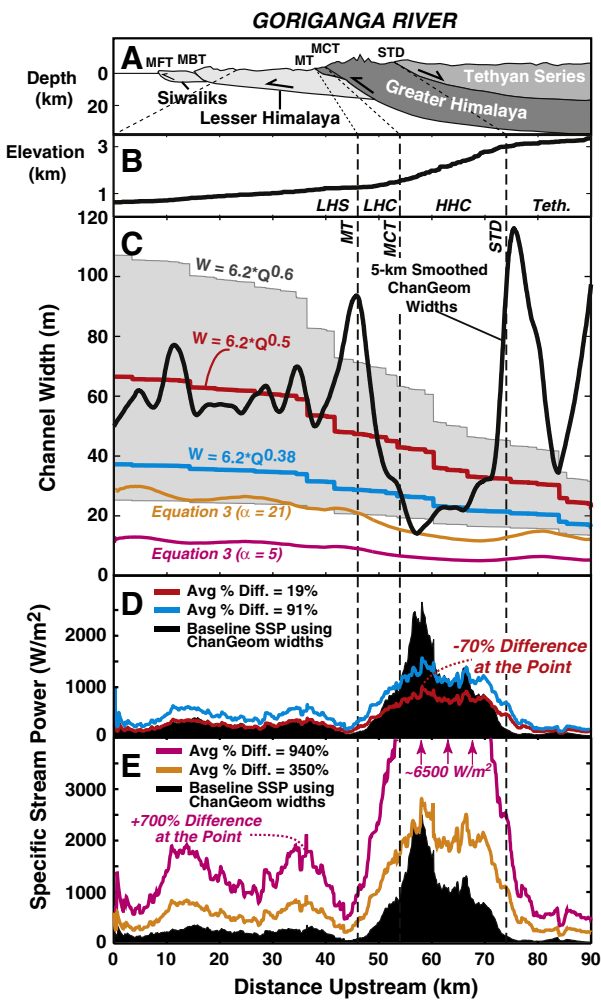


Fig. 7. Data from the Goriganga River, India showing A) the tectonic domains and major structures, as well as B) the longitudinal profile derived from the 90-m SRTM dataset (Fig. 1). C) Comparison of ChanGeom widths (black) with the range of discharge (Q) related power-law scaling exponents (Eq. (2)) from the literature (gray), the most commonly used power-law exponent (0.5 in red), an empirically derived power-law scaling from the Marsyandi River, Nepal (blue) (Craddock et al., 2007), and two different formulations of Eq. (3) (Finnegan et al., 2005) with width-to-depth ratios (α) equal to 5 (bedrock) and 21 (cobble) with a constant Manning's n of 0.04 (note that different parameters are used here than in Fisher et al., 2012). Note that the a value (6.2) from the Marsyandi River dataset is used as the hydrometeorology constant throughout in this analysis. D/E) Comparison of specific stream power values (ω) (Eq. (4)) using widths from part C with all other components held constant ($\rho g Q S$) across the datasets. LHS – Lesser Himalayan Sedimentary; LHC – Lesser Himalayan Crystalline; HHC – High Himalayan Crystalline; Tethy – Tethyan Series; MT – Munshyari Thrust; MCT – Main Central Thrust; STD – South Tibetan Detachment.

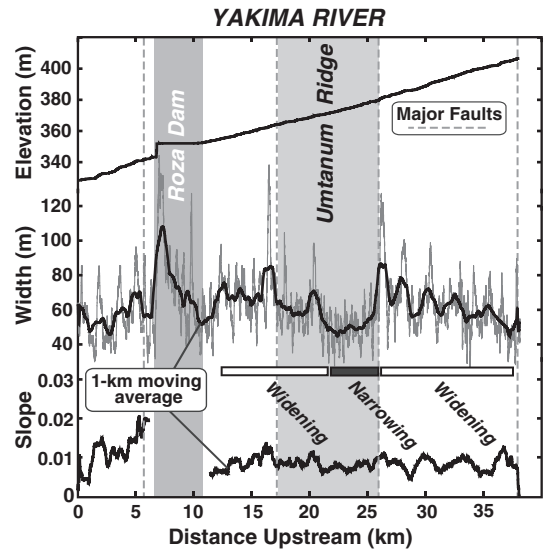


Fig. 8. Data from the Yakima River showing dynamic channel adjustment in response to variable tectonic regimes, with little change in channel slope. See Fig. 1 for an overview of the major structures.

(Eq. (4)). The traditional predictive models fail with regard to both the magnitude of width variability along the Goriganga River as well as the response of channel width to distinct tectonic and lithologic regimes (e.g., the High Himalayan Crystalline and Tethyan Series). Analysis of the power-law exponent (b) from Eq. (2) for each tectonic unit by Fisher et al. (2012) yielded values ranging from 4.4 in the Lesser Himalayan Crystalline (LHC) to -1.2 and -0.16 in the High Himalayan Crystalline (HHC) and Lesser Himalayan Series (LHS), respectively. Whereas the b value for the whole study reach is ~ 0.23 , more reasonable in the context of established values (Wohl and David, 2008), there are important processes and channel responses that are lost by “averaging” widths across landscapes characterized by such diverse structural, lithologic, and geomorphic forcings.

Historically, channel slope and its derivatives have provided a valuable first order proxy for relative rates of rock uplift and tectonic regime changes in orogenic environments (Seeber and Gornitz, 1983; Kirby and Whipple, 2012). Channel slope values along the Goriganga River (Fig. 7) illustrate this pattern well, where abrupt downstream changes correspond with major tectonic and lithologic boundaries. Changes in channel width can also reveal such boundaries independently of channel slope. The Yakima River canyon represents a prime example where channel width changes occur without concomitant changes in channel slope (i.e. knickpoints) or rock type as the river traverses a number of potentially active reverse faults and folds through Umtanum Ridge (Finnegan and Montgomery, 2003; Blakely et al., 2011) (Fig. 8). The independent response of channel width has been documented in both field and flume studies showing that variable tectonic rates are first accommodated by narrowing to a

width-to-depth threshold (~ 5 to 10) followed by increases in channel slope (Lavé and Avouac, 2001; Amos and Burbank, 2007; Finnegan et al., 2007; Yanites et al., 2010). The implication of this decoupling between channel width and slope, and given the fact that hydraulic radius and/or depth are almost never known, is that without both width and slope any fluvial signature of deformation along the Yakima River would be imperceptible in the channel slope values alone. In addition, channel width has been shown to dynamically adjust in response to perturbations in sediment supply in both flume and numerical studies (Finnegan et al., 2007; Attal et al., 2008), providing an additional research avenue where empirical use of the ChanGeom methodology could yield key insights from natural systems.

Theoretical and empirical field studies have documented channel slope responses to a host of forcings from landslide deposits (Korup et al., 2006; Ouimet et al., 2007) to vertical and slope-break knickpoints (Kirby and Whipple, 2012; Whipple et al., 2013) to folding and faulting regimes (Amos and Burbank, 2007; Whittaker et al., 2007; Yanites et al., 2010; Allen et al., 2011). However, quantifying both channel width and slope values could provide greater differentiation of landscape processes and transients than just slope alone. For example, minor landslides may be difficult to discern from knickpoints using channel slopes from coarse resolution DEMs where considerable noise may create stepped profiles regardless (Fig. 9). In the case of normal and thrust faults there should be distinct signatures in the channel width record that indicate relative movement and faulting style. A channel crossing a normal fault should exhibit excessive channel widening below the fault plane in response to the down-dropping of the hanging wall. This widening should be less exaggerated in the case of a channel traversing a thrust fault or growing

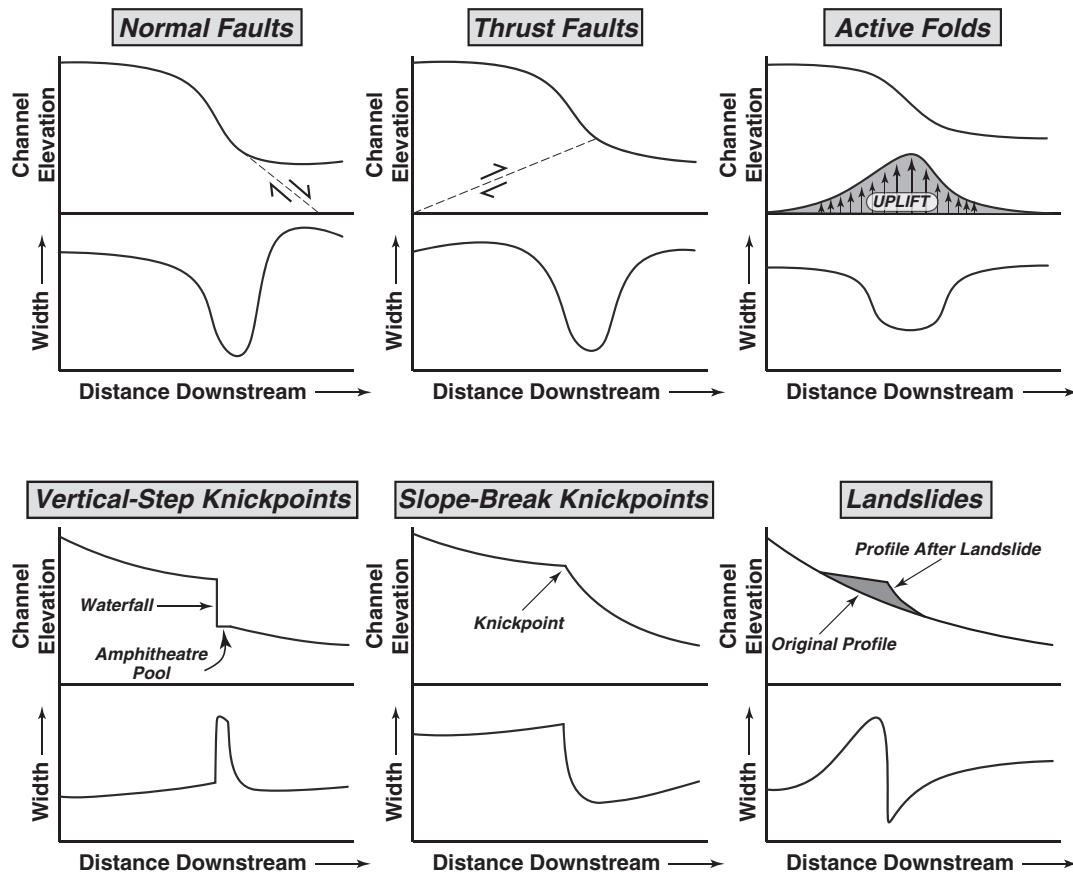


Fig. 9. Conceptual models of how channel width adjusts to different tectonic and geomorphic forcings. Changes in discharge are negligible for each panel such that the width profile is directly responding to the systematics of each channel profile forcing. These examples are idealized and we acknowledge that actual outcomes will depend on a host of factors including lithology, erodibility, discharge and sediment regimes, and forcing magnitudes. Also note that channel slope patterns will generally follow the inverse of the channel width profiles in these idealized cases (i.e. steepening of a channel will cause it to narrow).

fold. Utilizing high-spatial resolution channel widths should produce characteristic distributions, which when compared with channel slope analyses should allow much more information to be gleaned about the type and magnitude of different landscape forcings. Just as we can gain considerable information from the channel slope record, so too can we begin to further evolve our understanding of channel width signatures and overall planform geometry evolution in structurally, geomorphologically, and lithologically complex transient landscapes using the ChanGeom methodology and freely available high-spatial resolution imagery.

5. Conclusions

The development and widespread distribution of high-spatial resolution sensors and imagery over the last decade has created a vast opportunity for researchers concerned with channel form and process that has been largely unexploited to date, especially in tectonically active orogens. Here, we have presented a simple, fast methodology and toolbox (ChanGeom) to extract accurate channel planform geometry from freely available high-spatial resolution imagery in Google Earth and Bing Maps in ArcGIS, and proposed ways to drastically expand and improve current measurements of channel width, sinuosity, and slope in remote bedrock and lower drainage area channel systems. Examples from the Himalaya and North America emphasize both the information lost by using simple channel scaling metrics and the key insights that can be obtained from combining high-spatial resolution channel widths with channel slope datasets across large spans of river in tectonically active landscapes. Both the simplicity and the accuracy of the techniques presented here should newly ignite current debates about how channels adjust, scale, and record a host of landscape forcings (sediment, tectonic, lithologic, climatic, and geomorphic) as well as demonstrate the utility and accuracy of freely available high-spatial resolution imagery for improving quantitative measurements of surface processes.

Acknowledgments

This work was generously supported by a NASA Earth and Space Science Fellowship (NNX09A024H) to G.B. Fisher, and NASA (NNX08AG05G) and NSF grants (EAR0819874) to D.W. Burbank and B. Bookhagen. We thank Eric Kirby, Brian Yanites, and Will Ouimet for sharing their field data, Douglas Burbank for the helpful discussions, Ines Krauss for the help in digitizing, and Manfred Strecker for providing funds to travel to the University of Potsdam where this work was initiated. Lidar data for the Smith River were acquired from the Oregon Department of Geology and Mineral Industries (DOGAMI), while lidar datasets for the Yakima River and Dragon's Back Ridge were acquired through the NSF OpenTopography Facility (www.opentopography.org). ASTER GDEM V2 is a product of METI and NASA. Helpful reviews by Carl Legleiter, Thomas Farr, Tamlin Pavelsky, Brian Yanites, and an anonymous reviewer greatly improved this manuscript.

Appendix A. Supplementary data

The ChanGeom user's manual is available in the supplementary data for this article, with the newest versions and the Matlab source code (as well as future Python builds) available for download at the following web addresses:

<http://people.eri.ucsb.edu/~burch/Burchfisher/DATA.html>
<http://www.geog.ucsb.edu/~bodo/changeom>

Supplementary data to this article can be found online at <http://dx.doi.org/10.1016/j.geomorph.2013.04.011>.

References

- Allen, G.H., Barnes, J.B., Kirby, E., Pavelsky, T.M., 2011. Steady-state bedrock river response to tectonic and lithologic variations across active folds at the northwest Himalayan front. *EOS. Transactions of the American Geophysical Union* 92 (EP23C-0781).
- Amos, C.B., Burbank, D.W., 2007. Channel width response to differential uplift. *Journal of Geophysical Research* 112, F02010. <http://dx.doi.org/10.1029/2006JF000672>.
- Attal, M., Tucker, G.E., Whittaker, A.C., Cowie, P.A., Roberts, G.P., 2008. Modeling fluvial incision and transient landscape evolution: influence of dynamic channel adjustment. *Journal of Geophysical Research* 113, F03013. <http://dx.doi.org/10.1029/2007JF000893>.
- Bagnold, R.A., 1960. Sediment discharge and stream power, a preliminary announcement. *U.S. Geol. Surv. Circ. U.S.G.S.*, p. 23.
- Bagnold, R.A., 1977. Bed load transport by natural rivers. *Water Resources Research* 13, 303–312.
- Blakely, R.J., Sherrod, B.L., Weaver, C.S., Wells, R.E., Rohay, A.C., Barnett, E.A., Knepprath, N.E., 2011. Connecting the Yakima fold and thrust belt to active faults in the Puget Lowland, Washington. *Journal of Geophysical Research* 116, B07105. <http://dx.doi.org/10.1029/2010JB008091>.
- Bookhagen, B., Burbank, D.W., 2010. Toward a complete Himalayan hydrological budget: spatiotemporal distribution of snowmelt and rainfall and their impact on river discharge. *Journal of Geophysical Research* 115, F03019. <http://dx.doi.org/10.1029/2009JF001426>.
- Bookhagen, B., Strecker, M.R., 2012. Spatiotemporal trends in erosion rates across a pronounced rainfall gradient: examples from the southern Central Andes. *Earth and Planetary Science Letters* 327–328, 97–110.
- Breu, H., Gil, J., Kirkpatrick, D., Werman, M., 1995. Linear-time Euclidean distance transform algorithms. *IEEE Transactions on Pattern Analysis and Machine Intelligence* 17, 529–533.
- Constantine, J.A., Dunne, T., 2008. Meander cutoff and the controls on the production of oxbow lakes. *Geology* 36, 23–26.
- Craddock, W.H., Burbank, D.W., Bookhagen, B., Gabet, E.J., 2007. Bedrock channel geometry along an orographic rainfall gradient in the upper Marsyandi River valley in central Nepal. *Journal of Geophysical Research* 112, F03007. <http://dx.doi.org/10.1029/2006JF000589>.
- Duvall, A., Kirby, E., Burbank, D., 2004. Tectonic and lithologic controls on bedrock channel profiles and processes in coastal California. *Journal of Geophysical Research* — Earth Surface 109, F03002. <http://dx.doi.org/10.1029/2003JF000086>.
- Farr, T.G., Rosen, P.A., Caro, E., Crippen, R., Duren, R., Hensley, S., Kobrick, M., Paller, M., Rodriguez, E., Roth, L., Seal, D., Shaffer, S., Shimada, J., Umland, J., Werner, M., Oskin, M., Burbank, D., Alsdorf, D., 2007. The shuttle radar topography mission. *Reviews of Geophysics* 45, Rg2004. <http://dx.doi.org/10.1029/2005rg000183>.
- Finnegan, N.J., Montgomery, D.R., 2003. Geomorphic and seismic evidence for recent deformation in the Yakima Fold Belt between Ellensburg and Yakima, WA. *Geological Society of America Abstracts with Programs* 35, 512.
- Finnegan, N.J., Roe, G.H., Montgomery, D.R., Hallet, B., 2005. Controls on the channel width of rivers: implications for modeling fluvial incision of bedrock. *Geology* 33, 229–232.
- Finnegan, N.J., Sklar, L.S., Fuller, T.K., 2007. Interplay of sediment supply, river incision, and channel morphology revealed by the transient evolution of an experimental bedrock channel. *Journal of Geophysical Research* 112, F03S11. <http://dx.doi.org/10.1029/2006JF000569>.
- Fisher, G.B., Magilligan, F.J., Kaste, J.M., Nislow, K.H., 2010. Constraining the timescales of sediment sequestration associated with large woody debris using cosmogenic ⁷Be. *Journal of Geophysical Research* 115, F01013. <http://dx.doi.org/10.1029/2009JF001352>.
- Fisher, G.B., Bookhagen, B., Burbank, D.W., 2011. High-resolution channel widths and erosion along the entire Indus River. *EOS. Transactions of the American Geophysical Union* 92 (EP23C-0762).
- Fisher, G.B., Amos, C.B., Bookhagen, B., Burbank, D.W., Godard, V., 2012. Channel widths, landslides, faults, and beyond: the new world order of high-spatial resolution Google Earth imagery in the study of earth surface processes. In: Whitmeyer, S.J., De Paor, D.G., Bailey, J., Ornduff, T. (Eds.), *Google Earth, Virtual Globes, and Virtual Visualizations: Modern Approaches to Geoscience Inquiry and Research*. Geological Society of America Special Paper, 492, pp. 1–22. [http://dx.doi.org/10.1130/2012.2492\(01\)](http://dx.doi.org/10.1130/2012.2492(01)).
- Hack, J.T., 1957. Studies of longitudinal stream profiles in Virginia and Maryland. *U.S. Geological Survey Professional Paper* 294-B, 97.
- Hodges, K.V., 2000. Tectonics of the Himalaya and southern Tibet from two perspectives. *Geological Society of America Bulletin* 112, 324–350.
- Jansen, J.D., Codilean, A.T., Bishop, P., Hoey, T.B., 2010. Scale-dependence of lithological control on topography: bedrock channel geometry and catchment morphometry in western Scotland. *Journal of Geology* 118, 223–246.
- Jarvis, A., Reuter, H.I., Nelson, A., Guevara, E., 2008. Hole-filled Seamless SRTM Data V4. International Centre for Tropical Agriculture (CIAT) (available at <http://srtm.csi.cgiar.org>).
- Johnson, J.P., Whipple, K.X., 2007. Feedbacks between erosion and sediment transport in experimental bedrock channels. *Earth Surface Processes and Landforms* 32, 1048–1062. <http://dx.doi.org/10.1002/esp.1471>.
- Kirby, E., Ouimet, W., 2011. Tectonic geomorphology along the eastern margin of Tibet: insights into the pattern and processes of active deformation adjacent to the Sichuan Basin. In: Gloaguen, R., Ratschbacher, L. (Eds.), *Growth and Collapse of the Tibetan Plateau*. Geological Society, London, Special Publications, 353, pp. 165–188. <http://dx.doi.org/10.1144/SP353.9>.
- Kirby, E., Whipple, K., 2001. Quantifying differential rock-uplift rates via stream profile analysis. *Geology* 29, 415–418.

- Kirby, E., Whipple, K.X., 2012. Expression of active tectonics in erosional landscapes. *Journal of Structural Geology* 44, 54–75.
- Knighton, D.A., 1998. *Fluvial Forms and Processes*. Edward Arnold, London, UK.
- Korup, O., Strom, A.L., Weidinger, J.T., 2006. Fluvial response to large rock-slope failures: examples from the Himalayas, the Tien Shan, and the Southern Alps in New Zealand. *Geomorphology* 78, 3–21.
- Lam, L., Lee, S.-W., Suen, C.Y., 1992. Thinning methodologies—a comprehensive survey. *IEEE Transactions on Pattern Analysis and Machine Intelligence* 14, 869–885.
- Lavé, J., Avouac, J.-P., 2001. Fluvial incision and tectonic uplift across the Himalayas of central Nepal. *Journal of Geophysical Research—Solid Earth* 106, 26561–26591. <http://dx.doi.org/10.1029/2001JB000359>.
- Leopold, L., Maddock, T., 1953. The hydraulic geometry of stream channels and some physiographic implications. *U.S. Geological Survey Professional Paper* 252.
- Mackin, J.H., 1948. Concept of the graded river. *Geological Society of America Bulletin* 101, 1373–1388.
- Magilligan, F.J., 1992. Thresholds and the spatial variability of flood power during extreme floods. *Geomorphology* 5, 373–390.
- Manning, R., 1891. On the flow of water in open channels and pipes. *Institute of Civil Engineers of Ireland Transactions* 20, 161–207.
- Marcus, W.A., Fonstad, M.A., 2008. Optical remote mapping of rivers at sub-meter resolutions and watershed extents. *Earth Surface Processes and Landforms* 33, 4–24. <http://dx.doi.org/10.1002/esp.1637>.
- McKean, J., Nagel, D., Tonina, D., Bailey, P., Wright, C.W., Bohn, C., Nayegandhi, A., 2009. Remote sensing of channels and riparian zones with a narrow-beam aquatic-terrestrial lidar. *Remote Sensing* 1, 1065–1096. <http://dx.doi.org/10.3390/rs1041065>.
- Montgomery, D.R., Gran, K.B., 2001. Downstream variations in the width of bedrock channels. *Water Resources Research* 37, 1841–1846.
- O'Callaghan, J.F., Mark, D.M., 1984. The extraction of drainage networks from digital elevation data. *Computer Vision, Graphics and Image Processing* 28, 328–344.
- Ouimet, W., Whipple, K., Royden, L., Sun, Z., Chen, Z., 2007. The influence of large landslides on river incision in a transient landscape: eastern margin of the Tibetan Plateau (Sichuan, China). *Geological Society of America Bulletin* 119, 1462–1476. <http://dx.doi.org/10.1130/B26136.1>.
- Passalacqua, P., Belmont, P., Fofoula-Georgiou, E., 2012. Automatic geomorphic feature extraction from lidar in flat and engineered landscapes. *Water Resources Research* 48, W03528. <http://dx.doi.org/10.1029/2011WR010958>.
- Pavelsky, T.M., Smith, L.C., 2008. RivWidth: a software tool for the calculation of river widths from remotely sensed imagery. *IEEE Geoscience and Remote Sensing Letters* 5, 70–73.
- Potere, D., 2008. Horizontal positional accuracy of Google Earth's high-resolution imagery archive. *Sensors* 8, 7973–7981.
- Schumm, S.A., Khan, H.R., 1972. Experimental study of channel patterns. *Geological Society of America Bulletin* 83, 1755–1770.
- Schumm, S.A., Khan, H.R., Winkley, B.R., Robbins, L.G., 1972. Variability of river patterns. *Nature* 237, 75–76.
- Seeber, L., Gornitz, V., 1983. River profiles along the Himalayan Arc as indicators of active tectonics. *Tectonophysics* 92, 335–367.
- Slater, J.A., Heady, B., Kroenung, G., Curtis, W., Haase, J., Hoegemann, D., Shockley, C., Tracy, K., 2011. Global assessment of the new ASTER global digital elevation model. *Photogrammetric Engineering and Remote Sensing* 77, 335–349.
- Smith, L.C., 1997. Satellite remote sensing of river inundation area, stage, and discharge: a review. *Hydrological Processes* 11, 1427–1439.
- Smith, L.C., Pavelsky, T.M., 2008. Estimation of river discharge, propagation speed and hydraulic geometry from space: Lena River, Siberia. *Water Resources Research* 44, W03427.
- Snyder, N.P., Kammer, L.L., 2008. Dynamic adjustments in channel width in response to a forced diversion: Gower Gulch, Death Valley National Park, California. *Geology* 25, 187–190. <http://dx.doi.org/10.1130/G24217A.1>.
- Snyder, N.P., Whipple, K.X., Tucker, G.E., Merritts, D.J., 2003. Channel response to tectonic forcing: field analysis of stream morphology and hydrology in the Mendocino triple junction region, northern California. *Geomorphology* 53, 97–127.
- Stark, C.P., 2006. A self-regulating model of bedrock river channel geometry. *Geophysical Research Letters* 33, L04402. <http://dx.doi.org/10.1029/2005GL023193>.
- Stark, C.P., Barbour, J.R., Hayakawa, Y.S., Hattajji, T., Hovius, N., Chen, H., Lin, C.-W., Horng, M.-J., Xu, K.-Q., Fukahata, Y., 2010. The climatic signature of incised river meanders. *Science* 327, 1497–1501.
- Stølum, H.H., 1998. Planform geometry and dynamics of meandering rivers. *Geological Society of America Bulletin* 110, 1485–1498.
- Tewksbury, B.J., Dokmak, A.A.K., Tarabees, E.A., Mansour, A.S., 2012. Google Earth and geologic research in remote regions of the developing world: an example from the Western Desert of Egypt. In: Whittmeyer, S.J., De Paor, D.G., Bailey, J., Ornduff, T. (Eds.), *Google Earth, Virtual Globes, and Virtual Visualizations: Modern Approaches to Geoscience Inquiry and Research: Geological Society of America Special Paper*, 492, pp. 23–36. [http://dx.doi.org/10.1130/2012.2492\(02\)](http://dx.doi.org/10.1130/2012.2492(02)).
- Turowski, J.M., Lague, D., Crave, A., Hovius, N., 2006. Experimental channel response to tectonic uplift. *Journal of Geophysical Research* 111, F03008. <http://dx.doi.org/10.1029/2005JF000306>.
- Turowski, J.M., Lague, D., Hovius, N., 2007. Cover effect in bedrock abrasion: a new derivation and its implications for the modeling of bedrock channel morphology. *Journal of Geophysical Research* 112, F04006. <http://dx.doi.org/10.1029/2006JF000697>.
- Turowski, J.M., Lague, D., Hovius, N., 2009. Response of bedrock channel width to tectonic forcing: insights from a numerical model, theoretical considerations, and comparison with field data. *Journal of Geophysical Research* 114, F03016. <http://dx.doi.org/10.1029/2008JF001133>.
- Whipple, K.X., 2004. Bedrock rivers and the geomorphology of active orogens. *Annual Review of Earth and Planetary Sciences* 32, 151–185.
- Whipple, K., Snyder, N., Dollemeyer, K., 2000. Rates and processes of bedrock channel incision by the Upper Ukak river since the 1912 Novarupta Ash Flow in the Valley of Ten Thousand Smokes, Alaska. *Geology* 28, 835–838.
- Whipple, K.X., DiBiase, R.A., Crosby, B.T., 2013. Bedrock rivers. In: Shroder, John F. (Ed.), *Treatise on Geomorphology*, 9. Academic Press, San Diego, pp. 550–573.
- Whittaker, A.C., Cowie, P.A., Attal, M., Tucker, G.E., Roberts, G.P., 2007. Bedrock channel adjustment to tectonic forcing: implications for predicting river incision rates. *Geology* 35, 103–106.
- Wobus, C., Whipple, K.X., Kirby, E., Snyder, N., Johnson, J., Spyropoulou, K., Crosby, B., Sheehan, D., 2006a. Tectonics from topography: procedures, promise, and pitfalls. In: Willett, S.D., Hovius, N., Brandon, M.T., Fisher, D.M. (Eds.), *Tectonics, Climate, and Landscape Evolution: Geological Society of America Special Paper*, 398, pp. 55–74.
- Wobus, C.W., Tucker, G.E., Anderson, R.S., 2006b. Self-formed bedrock channels. *Geophysical Research Letters* 33, L18408.
- Wohl, E., David, G.C.L., 2008. Consistency of scaling relations among bedrock and alluvial channels. *Journal of Geophysical Research* 113, F04013.
- Yanites, B.J., Tucker, G.E., 2010. Controls and limits on bedrock channel geometry. *Journal of Geophysical Research* 115 (F4).
- Yanites, B.J., Tucker, G.E., Mueller, K.J., Chen, Y.G., Wilcox, T., Huang, S.Y., Shi, K.W., 2010. Incision and channel morphology across active structures along the Peikang River, central Taiwan: implications for the importance of channel width. *Geological Society of America Bulletin* 122, 1192–1208.